ELSEVIER

Journal of Molecular Catalysis A: Chemical 193 (2003) 185–196

JOURNAL OF MOLECULAR CATALYSIS A: CHEMICAL

www.elsevier.com/locate/molcata

Gas-phase hydrogenation of acetonitrile on zirconium-doped mesoporous silica-supported nickel catalysts

P. Braos-García, P. Maireles-Torres, E. Rodríguez-Castellón, A. Jiménez-López*

Departamento de Química Inorgánica, Cristalografía y Mineralogía, Facultad de Ciencias, Universidad de Málaga, Campus de Teatinos, 29071 Málaga, Spain

Received 23 April 2002; accepted 24 July 2002

Abstract

Nickel supported on zirconium-doped mesoporous silica catalysts, with varying nickel loadings (4–26 wt.%), were evaluated in the gas-phase hydrogenation of acetonitrile. Prior to the catalytic study, the catalysts were characterised by using XRD, XPS, HREM, H_2-TPR, N_2 adsorption–desorption at 77 K, H_2 and O_2 chemisorption and NH_3-TPD. The catalytic activity, at 408 K, was shown to be influenced by the incorporation procedure of nickel. The catalyst prepared by ion exchange being the one which exhibits the best catalytic performance. In the steady state, the turnover frequency value decreases from 0.020 to 0.004 mol CH_3CN converted at-g_{Ni}^{-1} s^{-1} as the nickel-supported content increases from 4 to 26 wt.%, but reaches the highest value (0.033 mol CH_3CN converted at-g_{Ni}^{-1} s^{-1}) for the nickel-exchanged catalyst. The selectivity, in all cases, is higher toward ethylamine (37–67 mol%), especially for higher nickel loadings. The studied catalysts deactivate during the catalytic reaction, and the extent of deactivation depends on both the nickel loading and the nickel incorporation method. However, the conversion and selectivity patterns of these catalysts can be completely restored after treatment with H_2 at 673 K for 1 h.

Keywords: Hydrogenation of acetonitrile; Supported nickel catalysts; Mesoporous solids; MCM-41; Zirconium oxide

1. Introduction

Lower aliphatic amines are valuable products widely used in the manufacture of medicinal, agricultural, textile, rubber and plastic chemicals. In recent years, gas-phase hydrogenation of nitriles has become an alternative method to produce amines beyond classical hydrogenation reactions in the liquid phase, in the presence of metallic catalysts at high temperatures and hydrogen pressures [1,2].

This new method seems to allow better control of the product selectivity [3–7], since a suitable choice of the support and the active phase can favour the formation of a particular amine. Thus, Verhaak et al. [5] have reported the influence of the acidity of the support of nickel-based catalysts on the selectivity in the hydrogenation of acetonitrile, demonstrating that basic supports favour the formation of the primary amine. These authors propose a mechanism whereby the active sites for hydrogenation are located on the metal, while the acid function, which catalyses the transamination reaction leading to secondary and tertiary amines, is situated on the support (a bifunctional mechanism). However, other authors [3,8] consider that all reaction steps which convert nitriles to different amines take place on the surface metal sites.

An important breakthrough in the field of porous inorganic solids was the discovery in the last decade

* Corresponding author. Tel.: +34-952131876; fax: +34-952132000.
E-mail address: ajimenezl@uma.es (A. Jiménez-López).

1381-1169/02/$ – see front matter
PII: S1381-1169(02)00454-5

of a new family of mesostructured molecular sieves, denominated as M41S [9,10]. Their high specific surface areas, uniform pore size distributions and tuneable acid/base and redox properties have opened new opportunities in sorption and catalysis [11,12]. Thus, for instance, the incorporation of zirconium into the hexagonal MCM-41 silica structure induces the creation of acid sites, which catalyse isopropanol dehydration [13] and are active in the vapour phase synthesis of alkylindoles from 2-ethylaniline and ethylene glycol [14]. Other authors have also reported the catalytic properties in liquid-phase oxidation with H_2O_2 of aniline [15] and with alkylperoxides of norbornylene and 2,6-di-*tert*-butylphenol [15]. This catalytic performance being attributed to the high dispersion of the zirconium species in the silica matrix. Furthermore, this mesoporous solid acting as catalytic support, ameliorates the degree of dispersion of chromium-supported oxide and its catalytic activity in the oxidative dehydrogenation of propane [16] and gives rise to cobalt-based catalysts which catalyse selective NO reduction at low temperatures using ammonia as reducing agent [17].

In this paper, we have used the hydrogenation of acetonitrile as a model reaction to study the catalytic behaviour of nickel supported on zirconium-doped mesoporous silica with different Ni loading in the hydrogenation of nitriles. The catalysts were characterised by chemical analysis, XRD, XPS, HREM, H_2-TPR, H_2 and O_2 chemisorption, N_2 adsorption and NH_3-TPD.

2. Experimental

A zirconium-doped mesoporous silica (Si/Zr molar ratio of 5) was prepared as described elsewhere [13] and used as a support for nickel catalysts. This support was impregnated with different nickel amounts (5–30 wt.% Ni), by using the incipient wetness method with aqueous solutions of nickel nitrate ($Ni(NO_3)_2{\cdot}6H_2O$, Aldrich). After calcination in air at 673 K for 4 h, the samples were reduced at 673 K in a H_2 flow of 50 ml min^{-1} for 60 min. These catalysts will be hereafter designated as SiZr-*x*Ni, where *x* is the weight percent of Ni. Moreover, a nickel-exchanged catalyst (SiZr-Niex) was prepared by putting the SiZr-5 support in contact with an aqueous solution of nickel acetate ($Ni(CH_3COO)_2{\cdot}4H_2O$, Aldrich) for 24 h, and repeating the treatment three times. Then, the sample obtained was treated in the same way as the other catalysts.

Ni content of the catalysts was determined by atomic absorption using a Perkin-Elmer 400 spectrometer. Powder X-ray diffraction patterns were obtained by using a Siemens D5000 diffractometer (Cu Kα source) provided with a graphite monochromator.

X-ray photoelectron spectroscopy (XPS) analyses were performed using a Physical Electronics 5700 instrument provided with a multichannel hemispherical electron analyser, the band-pass energy being 29.35 eV. The Mg Kα X-ray excitation source ($h\nu$ = 1253.6 eV) was at a power of 300 W and the pressure in the analysis chamber was maintained below 1×10^{-9} Torr during data acquisition. The binding energies (BE) were obtained with ±0.2 eV accuracy and charge compensation was carried out with the adventitious C 1s peak at 284.8 eV. Atomic concentrations were determined from elemental peak areas corrected for sensitivity differences. The sensitivity factors used are included in the PHI ACCESS data analysis software package. Before the XPS study, the samples were reduced in the catalytic reactor at 673 K, and maintained in a helium atmosphere until their displacement into the analysis chamber.

Hydrogen temperature-programmed reduction (H_2-TPR) experiments were carried out between 373 and 973 K, using a flow of Ar/H_2 (48 ml min^{-1}, 10 vol.% of H_2) and a heating rate of 10 K min^{-1}. Water produced in the reduction reaction was eliminated by passing the gas flow through a cold finger (193 K). The consumption of hydrogen was controlled by an on-line gas chromatograph provided with a TCD.

Textural parameters have been extracted from the N_2 adsorption–desorption isotherms at 77 K obtained using a conventional glass volumetric apparatus (outgassing at 473 K and 10^{-4} mbar overnight). Temperature-programmed desorption of ammonia (NH_3-TPD) was used to determine the total acidity of the catalysts. Before the adsorption of ammonia at 373 K, the samples were reduced at 673 K in a hydrogen flow (50 ml min^{-1}) for 60 min. The NH_3-TPD was performed between 373 and 1023 K, with a heating rate of 10 K min^{-1}. The evolved ammonia was analysed by on-line gas chromatograph (Shimadzu GC-14A) provided with a thermal conductivity detector.

The concentration of surface nickel atoms on the catalysts was established from hydrogen chemisorption at 298 K by using a conventional volumetric apparatus. A 450 mg of each precursor was reduced in situ at 673 K under a flow of hydrogen (heating rate of 10 K min^{-1}). Similarly, the amount of reduced nickel was evaluated by oxygen chemisorption at 673 K.

High resolution electron microscopy (HREM) was carried out with a Phillips CM-20 high-resolution transmission electron microscope equipped with an EDAX microanalysis system. Previously reduced samples were dispersed in *n*-heptane and suspended on a Cu grid of 3.5 mm in diameter.

The gas-phase hydrogenation of acetonitrile was performed in a flow system operating at atmospheric pressure. A tubular Pyrex reactor (27 cm length, 7 mm o.d. and 3.6 mm i.d.) was used. Prior to any measurement, 50 mg of catalyst (sieve fraction of 0.2–0.3 mm) was activated in situ at 673 K under a hydrogen flow for 60 min. After that, the hydrogen flow was bubbled through a saturator containing acetonitrile (Aldrich, 99.93+ wt.%, HPLC grade) at 273 K, thus resulting a feed with 7.1 mol% of acetonitrile, which was introduced into the reactor. The reactants and products were analysed by an on-line gas chromatograph equipped with a flame ionisation detector and a TRB-14 column. Tests were performed at 408 K, and a total flow rate of 150 ml min^{-1} was used.

The conversion is defined as

$$\text{Conversion (\%)} = 100 \times \frac{CH_3CN_{in} - CH_3CN_{out}}{CH_3CN_{in}}$$

The selectivities have been calculated from peak areas by considering the different sensitivity factors in the flame ionisation detector. The selectivity for the product *i* is defined as

$$\text{Selectivity}_i \text{ (mol\%)} = 100 \times \frac{(\text{corrected area})_i}{\text{sum of all corrected areas}}$$

A series of preliminary experiments consisting in varying parameters such as the size of the sieve fractions (0.2–0.3 and 0.3–0.4 mm) and both the catalyst mass and the gas flow rate at constant space velocity, were also carried out in order to rule out the existence of diffusional limitations under the experimental conditions used.

Temperature-programmed desorption studies were carried out after the catalyst deactivation by cooling to room temperature in the hydrogen flow containing acetonitrile, used previously as the feed. Then, the catalyst was heated under a flow of helium or hydrogen (50 ml min^{-1}), from room temperature to 673 K. During the heating process, the gas composition downstream of the reactor was measured continuously with an on-line gas chromatograph equipped with a flame ionisation detector and a TRB-14 column.

3. Results and discussion

3.1. Characterisation of catalysts

The incorporation of zirconium into a mesoporous silica produced a decrease in the long-range order as shown by the presence of an unique and broad reflection at low diffraction angle, but the reflection lines corresponding to ZrO_2 (tetragonal or monoclinic) were never observed. The d_{100} reflection of the support, assuming that a hexagonal structure is present, is barely modified after the impregnation or ion-exchange processes. However, the powder X-ray diffraction patterns of the SiZr-*x*Ni catalysts show the metallic nickel reflections at 1.76 and 2.03 Å, for Ni loading higher than 9 wt.%. The intensities of these peaks increase with the nickel loading (Fig. 1), revealing the formation of larger Ni particles. It must be considered that, taking into account the specific surface area of the support (793 $m^2\,g^{-1}$) and the cross-section of a nickel atom (0.065 nm^2), the support coverage is reached for nickel loading at values higher than 11.8 wt.%. Therefore, the tendency to form large metal particles will be more favourable for higher nickel contents, as revealed by XRD.

In order to get insights on both the surface composition and the chemical state of the active phase, X-ray photoelectron spectroscopy was employed in this study. Moreover, some information about the dispersion of the supported phase can also be obtained, under certain conditions, from the data concerning the atomic concentration of the elements present on the top surface of the sample. All the Ni 2p core level spectra are very similar, with an intense band corresponding to the Ni $2p_{3/2}$ peak centred at a BE of 853 eV, and two shoulders at higher energies, with BE values close

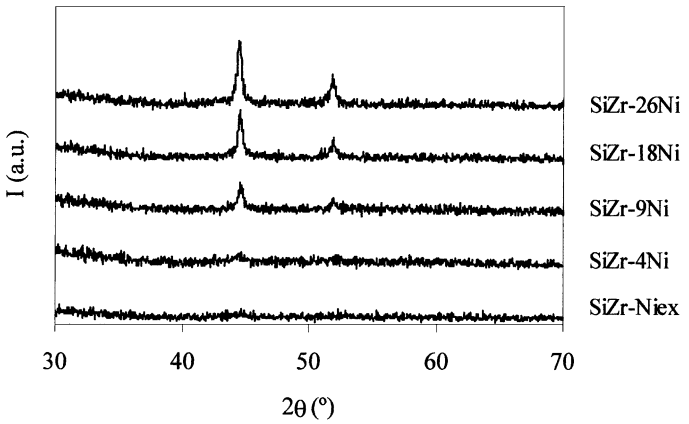

Fig. 1. Powder XRD patterns of Ni-supported catalysts.

to 856 and 862 eV. The band at 853 eV can be assigned to Ni^0, whereas the shoulder at 856 eV can be assigned to unreduced Ni(II) (Table 1 and Fig. 2). The band at 862 eV corresponds to the shake up satellite structure of Ni(II). It must be pointed out that, with this technique, only a proportion of the total metallic nickel is detected due to the existence of large metal particles, whose presence was already detected by XRD, and the surface sensitivity of the technique. The reverse happens with the unreduced nickel(II) which is easily detected since it is well dispersed as a consequence of its strong interaction with the support, whereas the metallic nickel tends to agglomerate. Moreover, since it was not possible to transport the reduced samples from the catalytic reactor to the spectrometer without exposure to air, the low percentage of metal nickel observed by XPS can also be attributed to a partial re-oxidation of the catalysts due to a short air exposure.

The photoelectronic Zr $3d_{5/2}$, Si 2p and O 1s signals of the zirconium-doped mesoporous silica, used as a support, are rather insensitive to the Ni coverage, i.e. 182.8 ± 0.6, 102.8 ± 0.6 and 532.8 ± 0.3 eV, respectively. It should be pointed out that oxygen from nickel oxide could not be distinguished from that of the support.

The comparison between the surface Ni/(Si + Zr) values calculated from XPS peak heights and atomic sensitivities and the corresponding bulk values can render information about the surface structure and the dispersion of the active phase. These values are also summarised in Table 1. It can be observed that the surface values are always lower than the corresponding bulk ratios, thus indicating that either unreduced nickel(II) migrates into the channels during the calcination at 673 K or that the degree of dispersion of nickel metal is low in this family of nickel-based catalysts.

Fig. 3 shows the H_2-TPR curves of the nickel-supported oxide catalysts, normalised by dividing the total amount of hydrogen consumed by the amount

Table 1
Binding energies (BE), surface and bulk Ni/(Si + Zr) molar ratio and percentage of Ni^0 as determined by XPS

Sample	Binding energy (eV)				Ni/(Si + Zr) molar ratio		Ni^0 (%)
	O 1s	Si 2p	Zr $3d_{5/2}$	Ni $2p_{3/2}$	Bulk	Surface	
SiZr-5	532.8	102.8	182.8	–	–	–	–
SiZr-Niex	533.1	103.2	182.8	852.9, 855.9	0.085	0.055	29
SiZr-4Ni	532.7	102.8	182.2	852.7, 855.7	0.053	0.037	38
SiZr-9Ni	533.1	103.2	182.8	852.9, 855.5	0.119	0.092	35
SiZr-18Ni	532.6	102.6	182.6	852.5, 855.3	0.275	0.207	31
SiZr-26Ni	533.0	103.4	183.1	852.9, 855.5	0.468	0.327	29

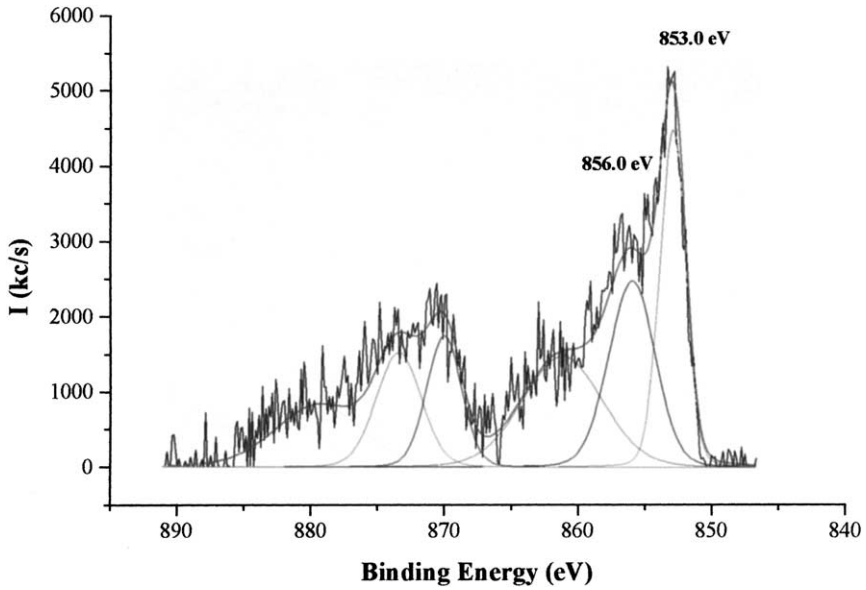

Fig. 2. Ni 2p XPS spectra of the SiZr-4Ni catalyst.

of nickel on each catalyst. It can be observed that the reduction of nickel-supported oxide is, in all cases, accomplished in two steps, pointing out the existence of Ni(II) in different environments. An intense and broad band, which in some cases allows two maxima to be distinguished, is observed between 513 and 673 K, which is more intense for higher nickel loading. Thus, taking into account that bulk NiO is reduced in one step at temperatures close to 500 K, this hydrogen consumption could be assigned to the reduction of large NiO particles. Hydrogen is also consumed at higher temperatures (673–873 K), also giving rise to a very broad band, which decreases in intensity as the nickel loading increases. This reduction pattern suggests the existence of a reducible form of NiO at low temperature, whereas the decreased reducibility of the NiO could be due to chemical interaction with the support of smaller nickel oxide particles. Similar patterns and trends as a function of the Ni loading have been found for NiO supported on α-Al_2O_3 [18]. However, the profile of the nickel-exchanged catalyst is different, since only a broad band centred at 723 K is observed, whereas the hydrogen consumption at temperatures lower than 573 K is negligible. This specific behaviour confirms the existence of nickel(II) species on this catalyst strongly interacting with the support, and also being difficult to reduce. This agrees very well with the results obtained by XPS and H_2 chemisorption (vide infra). Since the temperature at which the reduction of the nickel-exchanged sample takes place is very close to the reduction peak at high temperatures found for the nickel-supported oxide catalysts, there would seem to be a fraction of nickel(II) that could be interacting with the exchange sites of the support.

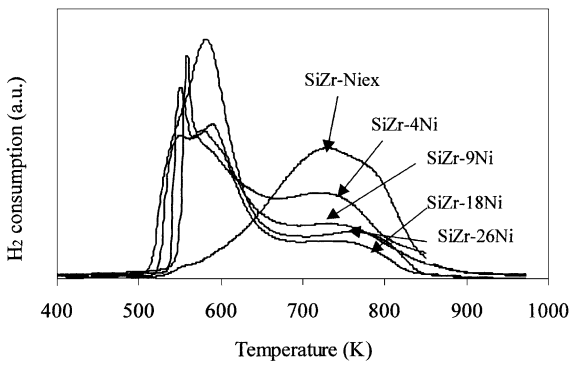

Fig. 3. Normalized H_2-TPR profiles of nickel-supported catalysts before reduction.

A similar trend in the XRD patterns and the H_2-TPR curves has been found for 10 wt.% Ni-loaded silica catalysts [19] in the study of the influence of the

Table 2
Chemical composition, textural and acidic characteristics of the support and the nickel-based catalysts

Sample	Ni (wt.%)	S_{BET} ($m^2\,g^{-1}$)	V_p ($cm^3\,g^{-1}$)	NH_3-TPD ($\mu mol\ NH_3\ g^{-1}$)	CN analysis spent catalysts (wt.%)	
					C	N
SiZr-5	–	793	0.577	1055	–	–
SiZr-Niex	6.52	398	0.445	830	3.40	0.62
SiZr-4Ni	4.35	468	0.337	565	5.86	2.21
SiZr-9Ni	8.63	489	0.336	443	4.94	0.84
SiZr-18Ni	17.80	430	0.291	374	4.14	0.62
SiZr-26Ni	26.10	406	0.272	326	3.43	0.59

preparation method (incipient wetness impregnation, ion exchanged and precipitation–deposition) and the nature of the support on the stability of the nickel dispersion. These authors reported the virtual absence of diffraction lines corresponding to NiO and the high reduction temperatures of the nickel species of the exchanged sample.

As regards the textural characteristics of these nickel oxide-based precursors (Table 2), the specific surface areas and the pore volumes are lower than those corresponding to the support ($S_{BET} = 793\,m^2\,g^{-1}$ and $V_p = 0.577\,cm^3\,g^{-1}$), whereas the pore size distributions are similar to that of the support, with only a single maximum centred at 2.2 nm. Therefore, the results obtained from N_2 adsorption and XRD reveal that the decrease in the S_{BET} values is not only due to the increment of the specific weight of the sample, but also to the presence, after the impregnation process, of large NiO particles on the support, which probably block the access of nitrogen molecules to the mesoporous network. In the case of the nickel-exchanged catalyst, the presence of a high number of small nickel oxide particles (and hence not detected by XRD) and a partial modification of the mesoporous structure during the ion-exchange process in aqueous solution could be responsible of its lowest specific surface area. The latter phenomenon is a well known drawback of the family of mesoporous MCM-41 solids.

On the other hand, the advantage of a zirconium-doped mesoporous silica support in comparison to a pure mesoporous silica has been largely justified in several papers [13–17], and, among others things, this advantage lies in its higher acidity (1055 μmol NH_3 desorbed g^{-1}), and its still high specific surface area. The total acidity of the Ni^0-supported catalysts, as determined by NH_3-TPD, decreases with the amount of nickel incorporated, again indicating that the nickel particles either mask surface acid sites or that the pore blockage impedes the access of the ammonia molecules to acid sites. However, the high acidity value found for the nickel-exchanged catalyst is noteworthy (830 $\mu mol\ NH_3\ g^{-1}$), and would indicate the contribution to acidity of the high proportion of unreduced nickel species, since the stability of coordination compounds formed by nickel(II) and ammonia is well known.

The degree of nickel dispersion was evaluated from the H_2 chemisorption data by assuming that the ratio of the total amount of adsorbed hydrogen atoms to exposed Ni atoms is 1:1. The reduction percentage, as determined by oxygen chemisorption at 673 K, reveal that at the reduction temperature used for this family of catalysts (673 K), an almost complete reduction of the nickel-supported catalysts ($Ni^0/Ni > 90\%$) is achieved, whereas the low degree of reduction of the nickel-exchanged catalyst (67%) again reflects the strong interaction between the exchanged nickel species and the support (Table 3). The values of the nickel-supported catalysts agree well with those reported by Hoang-Van et al. [20] for nickel supported on silica and titania (12 wt.%), where reduction percentages ranging between 81 and 97% are found after reduction at 573 and 773 K. However, the hydrogen chemisorption is very different, because the SiZr-9Ni catalyst, with a similar nickel content, chemisorbed a small amount of hydrogen (9.5 $\mu mol\,g^{-1}$) in comparison to the above mentioned catalysts whose adsorption exceeds the value of 72 $\mu mol\,g^{-1}$. The metal particle sizes derived from H_2 chemisorption do not match very well with the values calculated from the line broadening analysis of the corresponding XRD patterns.

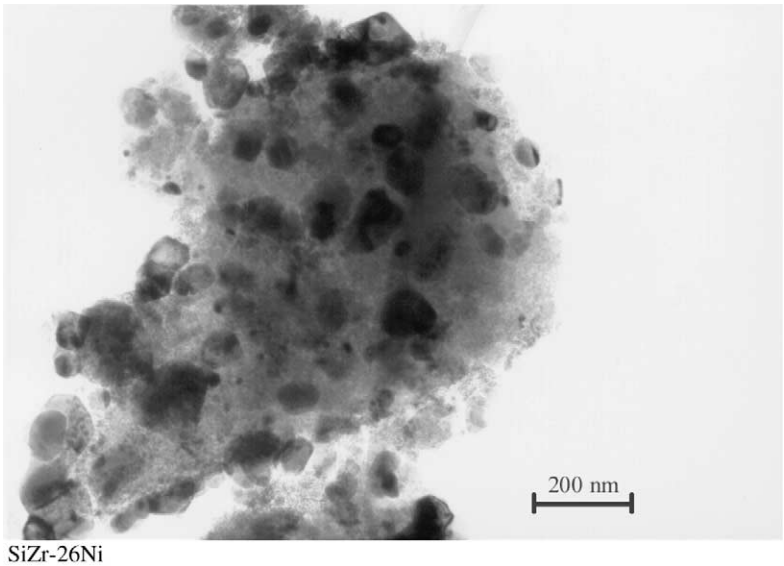

SiZr-26Ni

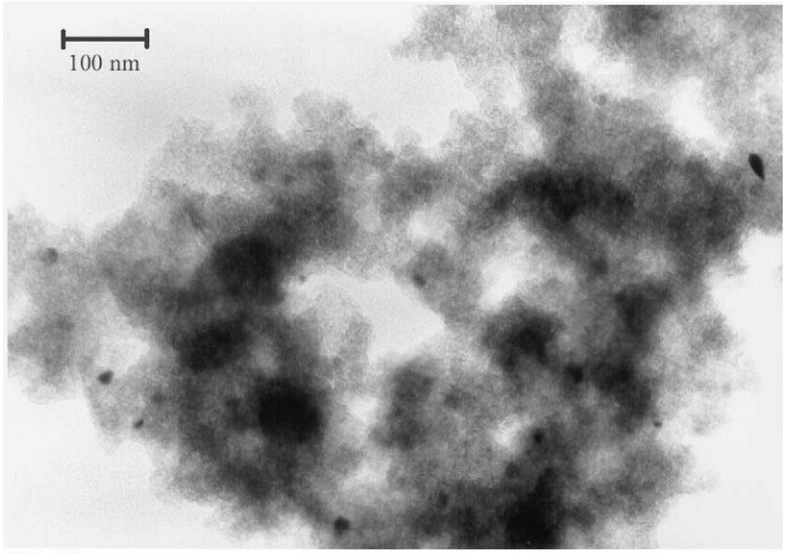

SiZr-Niex

Fig. 4. Transmission electron micrographs of SiZr-Niex and SiZr-26Ni catalysts.

A more realistic vision of the metallic particles and their distribution can be furnished by high-resolution transmission electron microscopy. Thus, the micrographs displayed in Fig. 4 show the presence of metal particles of very different sizes, pointing to a heterogeneous distribution of metal sizes, which values increases as the concentration of nickel does it. However, the differences between the nickel-exchanged catalyst and a nickel-impregnated catalyst, SiZr-26Ni, are evident. By comparing the metal particle sizes deduced from hydrogen chemisorption with those observed by TEM (Table 3), it is found that, bearing in mind their heterogeneous distribution, the former fall very close to the range determined from the micrographs.

Table 3
Properties of the nickel-supported catalysts (percentage of nickel reduction obtained from O_2 chemisorption)

Catalyst	Ni^0/Ni total (%)	H_2 chemisorbed (μmol H_2 g^{-1})	D (%)	Metal area (m^2 g_{Ni}^{-1})	d (nm)		
					H_2	TEM	XRD
SiZr-Niex	67	25.8	6.95	45.1	6	7–20	n.d.
SiZr-4Ni	90	5.9	1.76	11.4	34	20–40	n.d.
SiZr-9Ni	97	9.5	1.33	8.7	48	45–75	24
SiZr-18Ni	95	18.1	1.25	8.1	50	45–90	24
SiZr-26Ni	92	25.8	0.96	6.3	63	55–90	27

3.2. Catalytic results

This family of nickel-based catalysts was tested in the gas-phase hydrogenation of acetonitrile. The detected reaction products were ethylamine (EA), diethylamine (DEA), triethylamine (TEA), *N*-ethylethylimine (EEI), methane (CH_4) and traces of ethane. Previous tests carried out have demonstrated that, as expected, low space velocities and high H_2/acetonitrile ratios increase the acetonitrile conversion, as well as high reaction temperatures, although at temperatures higher than 413 K, the appearance of cracking products limits the yield in amines and the catalysts deactivate faster due to coke deposition.

By considering these previous results, the following experimental conditions were chosen: $T = 408$ K, $F/W = 50\,cm^3\,g^{-1}\,s^{-1}$, H_2/CH_3CN molar ratio = 13.2. Under these experimental conditions, these catalysts are very active in this catalytic reaction, but all of them deactivate during the course of the catalytic reaction. This deactivation depends on the nickel loading and the nickel incorporation method (impregnation or ion-exchange). Deactivation of catalysts in the acetonitrile hydrogenation has already been reported for reduced Ni-Mg-Al hydrotalcites [21] and nickel supported on silica [22].

Table 4 compiles the rates of the catalytic process at different points in the reaction (initial, just before deactivation and in the steady state), as well as the conversion and selectivity values for all the catalysts in the steady state. Initial acetonitrile conversion values, calculated by extrapolating to zero time, are 100% in all cases, but very different product distributions are found depending on the catalyst (Fig. 5). Thus, EA, DEA and TEA are the main reaction products, but with the exception of SiZr-4Ni, methane is also detected. The behaviour of the SiZr-26Ni is noteworthy, because at the beginning of the catalytic reaction only methane is detected.

The SiZr-4Ni and SiZr-9Ni catalysts quickly deactivate (after 1 h of time-on-stream (TOS)) whereas, interestingly, the catalyst prepared by ion-exchange, SiZr-Niex, maintains a very high conversion (>89%) after 19 h of TOS (Fig. 6).

The study of the variation of acetonitrile conversion and selectivity as a function of TOS reveals that the selectivity towards EA increases as the conversion decreases, as observed for the SiZr-26Ni catalyst in Fig. 7. This fact is concomitant with a slight decrease in the selectivities to DEA and TEA.

In the case of the selectivity values in the steady state, at conversions lower than 31% (Table 4), the

Table 4
Catalytic properties of the nickel-supported catalysts in the hydrogenation of acetonitrile at 408 K

Catalyst	Rate (μmol g^{-1} s^{-1})			Conversion steady state (mol%)	Product selectivity in the steady state (mol%)			
	Initial	Before deactivation	Steady state		EA	DEA	TEA	EEI
SiZr-Niex	119.8	106.6	36.9	30.8	59.8	30.6	1.6	8.0
SiZr-4Ni	123.5	113.6	15.1	12.2	36.5	37.5	13.0	13.0
SiZr-9Ni	122.6	111.6	15.8	12.9	39.6	39.4	4.7	16.3
SiZr-18Ni	121.3	111.6	16.4	13.5	62.0	27.8	0.0	10.2
SiZr-26Ni	121.2	108.4	19.3	15.9	67.0	25.3	0.0	7.6

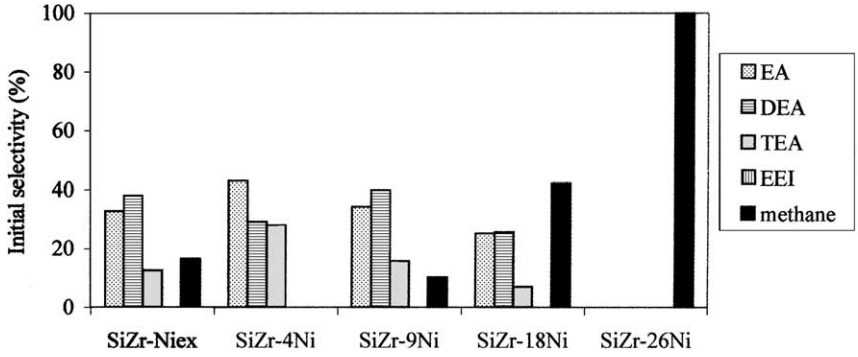

Fig. 5. Initial selectivity values in the gas-phase hydrogenation of acetonitrile on nickel-based zirconium-doped mesoporous silica catalysts at 408 K.

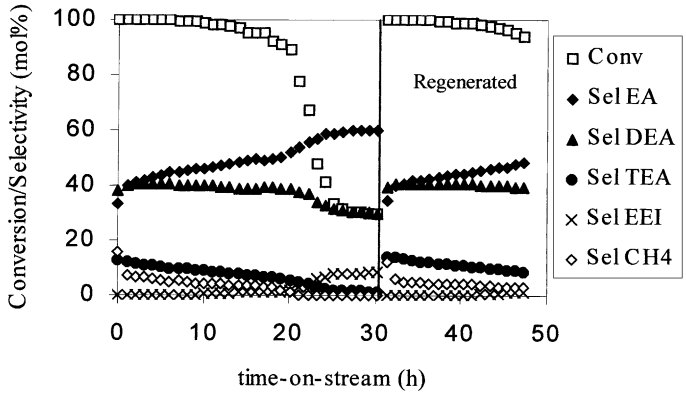

Fig. 6. Variation of the conversion and selectivity in the gas-phase hydrogenation of acetonitrile as a function of TOS on the SiZr-Niex catalyst at 408 K.

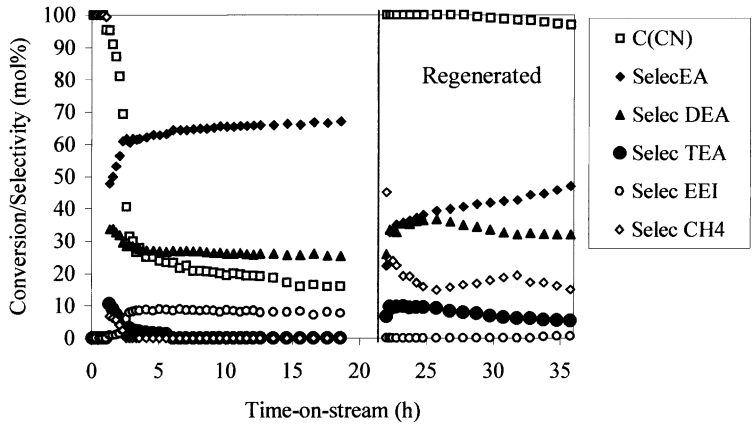

Fig. 7. Conversion and selectivity values in the gas-phase hydrogenation of acetonitrile as a function of TOS on the SiZr-26Ni catalyst at 408 K.

main reaction product is EA with a selectivity higher than 36%, whereas the formation of TEA is limited to values lower than 13%, and in some cases its formation is nil. Moreover, in general, there is an increment in the selectivity to EA with Ni loading, which reaches a value of 67% for SiZr-26Ni, but the selectivity towards the condensation products diminishes. Moreover, the formation of EEI as by-products is mainly detected at low conversion values, according to the results reported by Medina-Cabello et al. [21].

It would be expected that a more acid catalyst favours the condensation reactions leading to higher amines. Therefore if we consider the acid–base interaction between the support and the different molecules present in the reaction media with increasing basicity (CH_3CN < EA < TEA < DEA [23]), the selectivity to the condensation products may be enhanced as the acidity increases. The experimental data in the present work seem to support this assumption, since there are significant differences in the selectivity between the catalysts with low and high nickel contents, more condensation products appearing in the catalysts with low nickel loading, i.e. the more acidic catalyst.

On the other hand, in order to get insights into the causes of the deactivation process, the spent catalysts were analysed. The carbon and nitrogen percentages found are, in all cases, higher than 3.4 and 0.6 wt.%, respectively, the highest values of coke corresponding to the catalysts impregnated with the lowest Ni contents, SiZr-4Ni and SiZr-9Ni (Table 2). These catalysts are also those which lose their catalytic activity more quickly. Moreover, it is noteworthy that these catalysts are also the most acidic, indicating that a correlation between the deactivation and the presence of strong acid sites is established. These results contrast with the behaviour found for the ion-exchanged catalyst, which, in spite of being the most acidic, maintains a high catalytic activity for a long time (19 h of TOS). This apparent contradiction could be explained by taking into account that on the exchanged catalyst the important fraction of unreduced nickel(II) is responsible for its high acidity and the experimental data suggest that these unreduced Ni(II) ions do not participate in the catalytic reaction. Moreover, it can be held that the presence of these Ni(II) ions avoids the fast deactivation of the metal centres.

It has been previously demonstrated that the deactivation of nickel-supported catalysts is due to both the presence of carbonaceous residues such as surface nickel carbide and partly dehydrogenated acetonitrile species [22]. Nevertheless, the C/N molar ratios found in the deactivated catalysts can not completely rule out the existence of strongly adsorbed triethylamine molecules which may cover the active sites, resulting in the deactivation of the catalysts, as suggested by Arai et al. [24] in the study of platinum-supported catalysts.

More information about the deactivation process was obtained by treating a spent catalyst to a thermal programmed desorption under a nitrogen or helium flow. The results obtained by using helium as the carrier gas (Fig. 8) reveal a strong desorption of acetonitrile from the onset of the desorption process. This desorption may correspond to acetonitrile physisorbed on the catalyst surface, since the catalyst is cooled down from the reaction temperature to room temperature under the reaction feed. Moreover, a small amount of acetonitrile is also evolved at higher temperatures (close to 475 K), which could be assigned to molecules strongly retained by the metal particles, together with EEI and TEA. However, it is noteworthy that the attempt to regenerate the catalyst by flowing helium at 673 K was unsuccessful, the catalyst being completely deactivated. It can be assumed that this thermal treatment under an inert atmosphere might favour the sinterisation of the metal particles and the formation of more coke and nickel carbide/nitride by pyrolysis of the adsorbed molecules. In contrast, when the TPD of the spent catalyst is carried out under hydrogen, the profile is very different (Fig. 9), because a very intense peak corresponding to methane is observed at 510 K, indicating that the carbonaceous residues are eliminated by hydrogenation. The amount of acetonitrile evolved is reduced and different amount of EEI, DEA and TEA are detected. But, interestingly, the catalyst, after hydrogen treatment, completely recovers its initial activity. In general, the catalytic activity of this family of catalysts can be almost completely restored after treatment under a hydrogen flow at 673 K for 1 h.

By comparing the product distributions and the acetonitrile conversions just before the deactivation process and after regeneration, they are found to be very similar. This behaviour reveals that the catalysts are modified during the catalytic reaction, perhaps the number and nature of nickel particles and acid sites should be changed, and the strongest acid sites are

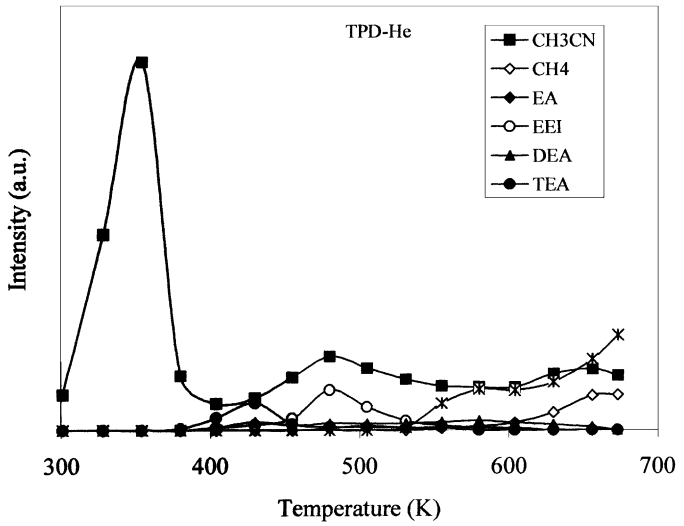

Fig. 8. TPD curves of the spent SiZr-Niex catalyst carried out under helium flow.

eliminated by the irreversible deposit of coke. This fact will agree with the negligible amount of methane produced on the regenerated catalysts. Therefore, it is worth emphasising the high catalytic activity, the easy regeneration of this family of catalysts and, in particular, the high stability of the nickel-exchanged catalyst and the impregnated catalyst with the highest amount of nickel, SiZr-26Ni, which, after regeneration, maintains their catalytic activity after more than 10 h of TOS.

On the other hand, a still controversial aspect in the study of the gas-phase hydrogenation of acetonitrile is establishing that the general mechanism is. It has been previously commented that different mechanisms have been put forward in the literature in order to explain the different experimental results published. Recently, we have studied this catalytic reaction using nickel supported on alumina and alumina/gallium oxide pillared tin(IV) phosphates, and the results can be well explained assuming that both the hydrogenation

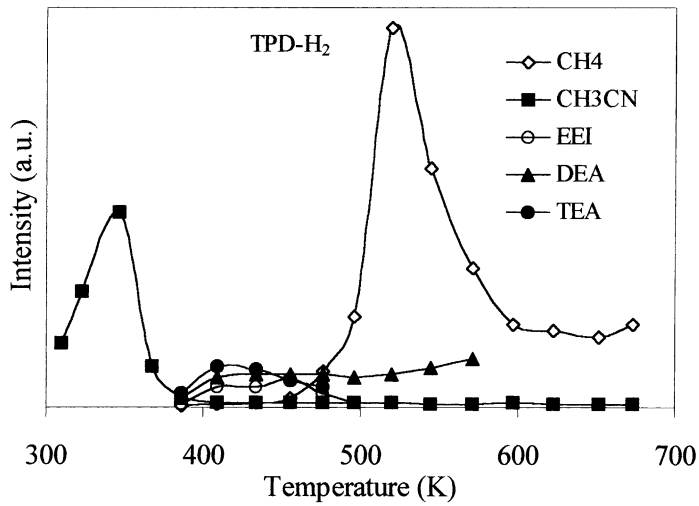

Fig. 9. TPD curves of the spent SiZr-Niex catalyst carried out under hydrogen flow.

and condensation reactions take place on the metal particles [25]. However, the catalytic behaviour of the nickel-supported catalysts described in the present work, with a lower selectivity to the higher amines for the catalyst with lower acidity, could indicate that the condensation reactions take place on the acid sites located on the support. Nevertheless, it seems that further experimental work is necessary to shed more light on the mechanism operating in the gas-phase hydrogenation of acetonitrile with this family of catalysts.

4. Conclusions

In conclusion, from the present catalytic study, it could be inferred that the use of porous solids, belonging to the MCM-41 family, with a high surface area, pore sizes in the mesoporous range and tuneable acidity, acting as supports for metal particles, gives rise to easily regenerable catalysts with very high catalytic activity in the gas-phase hydrogenation of acetonitrile.

Acknowledgements

The financial support for this research was obtained under the project MAT97-906 (CICYT, Spain), to which we are very grateful.

References

[1] K. Weissermel, H.J. Arpe, Industrial Organic Chemistry, Verlag Chemie, Berlin, 1978.
[2] M. Grayson (Ed.), Kirk-Othmer Encyclopedia of Chemical Technology, vol. 2, 2nd ed., Wiley/Intersciences, New York, 1983.
[3] Y. Huang, W.M.H. Sachtler, Appl. Catal. A 182 (1999) 365.
[4] C.V. Rode, M. Arai, M. Shirai, Y. Nishiyama, Appl. Catal. A 148 (1997) 405.
[5] M.J.F.M. Verhaak, A.J. van Dillen, J.V. Geus, Catal. Lett. 26 (1994) 37.
[6] F. Medina, R. Dutartre, D. Tichit, B. Coq, N.T. Dung, P. Salagre, J.E. Sueiras, J. Mol. Catal. A: Chem. 119 (1997) 201.
[7] Y. Huang, V. Adeeva, W.M.H. Sachtler, Appl. Catal. A 196 (2000) 73.
[8] M. Arai, Y. Takada, Y. Nishiyama, J. Phys. Chem. B 102 (1998) 1968.
[9] C.T. Kresge, M.H. Leonowicz, W.J. Roth, J.C. Vartuli, J.S. Beck, Nature 359 (1992) 710.
[10] J.S. Beck, J.C. Vartuli, W.J. Roth, M.E. Leonowicz, C.T. Kresge, K.D. Schmitt, C.T.W. Chu, D.H. Olson, E.W. Sheppard, S.B. McCullen, J.B. Higgins, J.L. Schlenker, J. Am. Chem. Soc. 114 (1992) 10834.
[11] A. Corma, Chem. Rev. 97 (1997) 2373.
[12] U. Ciesla, F. Schüth, Microporous Mesoporous Mater. 27 (1999) 131.
[13] D.J. Jones, J. Jiménez-Jiménez, A. Jiménez-López, P. Maireles-Torres, P. Olivera-Pastor, E. Rodríguez-Castellón, J. Rozière, Chem. Commun. (1997) 341.
[14] A.O. Bianchi, M. Campanati, P. Maireles-Torres, E. Rodríguez-Castellón, A. Jiménez-López, A. Vaccari, Appl. Catal. A 220 (2001) 105.
[15] S. Gontier, A. Tuel, Appl. Catal. A 143 (1996) 125.
[16] A. Jiménez-López, E. Rodríguez-Castellón, P. Maireles-Torres, L. Díaz, J. Mérida-Robles, Appl. Catal. A 218 (2001) 295.
[17] R. Moreno-Tost, J. Santamaría-González, P. Maireles-Torres, E. Rodríguez-Castellón, A. Jiménez-López, Appl. Catal. B 38 (2002) 51.
[18] J.T. Richardson, M. Lei, B. Turk, K. Foster, M.V. Twigg, Appl. Catal. A 110 (1994) 217.
[19] A. Gil, A. Díaz, L.M. Gandía, M. Montes, Appl. Catal. A 109 (1994) 167.
[20] C. Hoang-Van, Y. Kachaya, S.J. Teichner, Y. Arnaud, J.A. Dalmon, Appl. Catal. 46 (1989) 281.
[21] F. Medina-Cabello, D. Tichit, B. Coq, A. Vaccari, N.T. Dung, J. Catal. 167 (1997) 142.
[22] M.J.F.M. Verhaak, A.J. van Dillen, J.W. Geus, J. Catal. 143 (1993) 187.
[23] A. Streitwieser, C.H. Heathcock, Química Orgánica, McGraw-Hill Interamericana, 1989, p. 756.
[24] M. Arai, Y. Takada, T. Ebina, M. Shirai, Appl. Catal. A 183 (1999) 365.
[25] P. Braos-García, P. Maireles-Torres, E. Rodríguez-Castellón, A. Jiménez-López, J. Mol. Catal. A: Chem. 168 (2001) 279.